AGU PUBLICATIONS

JGR

Journal of Geophysical Research: Atmospheres

RESEARCH ARTICLE
10.1002/2014JD021914

Key Points:
- AIE of aircraft soot on cirrus clouds is from -0.35 W m^{-2} to 0.09 W m^{-2}
- The uncertainty is caused by the background sulfate and dust number

Supporting Information:
- Readme
- Text S1
- Figure S1
- Figure S2
- Figure S3

Correspondence to:
C. Zhou,
zhouc@umich.edu

Citation:
Zhou, C., and J. E. Penner (2014), Aircraft soot indirect effect on large-scale cirrus clouds: Is the indirect forcing by aircraft soot positive or negative?, *J. Geophys. Res. Atmos.*, *119*, 11,303–11,320, doi:10.1002/2014JD021914.

Received 21 APR 2014
Accepted 8 SEP 2014
Accepted article online 10 SEP 2014
Published online 1 OCT 2014

Aircraft soot indirect effect on large-scale cirrus clouds: Is the indirect forcing by aircraft soot positive or negative?

Cheng Zhou[1] and Joyce E. Penner[1]

[1]Department of Atmospheric, Oceanic, and Space Sciences, University of Michigan, Ann Arbor, Michigan, USA

Abstract The indirect effect of aircraft soot on cirrus clouds is subject to large uncertainties due to uncertainty in the effectiveness of aircraft soot acting as heterogeneous ice nuclei (IN) and the complexity caused by background ice nucleation, which introduces two major competing ice nucleation mechanisms: homogeneous freezing that generally produces more abundant ice particles and heterogeneous nucleation that generally produces fewer ice particles. In this paper, we used the coupled Community Atmosphere Model version 5.2 (CAM5)/IMPACT model to estimate the climate impacts of aircraft soot acting as IN in large-scale cirrus clouds. We assume that only the aircraft soot particles that are preactivated in persistent contrail cirrus clouds are efficient IN. Further, we assume that these particles lose their ability to act as efficient IN when they become coated with three monolayers of sulfate. We varied the background number concentration of sulfate aerosols allowed to act as homogeneous ice nucleation sites as well as the dust concentrations that act as heterogeneous ice nuclei to examine the sensitivity of the forcing by aircraft soot to the background atmosphere. The global average effect can range from a high negative (cooling) rate, -0.35 W m^{-2}, for the high sulfate/low dust case to a positive (warming) rate, +0.09 W m^{-2}, for the low sulfate/low dust case (default CAM5 setup) when approximately 0.6% of total aviation soot acts as IN. The net negative forcing is caused by the addition of IN to a background atmosphere that is dominated by homogeneous nucleation (mainly in the tropic Indian Ocean, Central America, and North Atlantic Ocean). The forcings can be all positive, about +0.11 to +0.21 W m^{-2}, when the background atmosphere is dominated by pure heterogeneous ice nucleation.

1. Introduction

Aviation emissions contribute to the radiative forcing of climate [*Lee et al.*, 2009]. Aviation-induced cirrus cloud cover is thought to arise from two different mechanisms. First, emissions from aviation activities can form linear contrails, which may have a global coverage of ~0.07% [*Duda et al.*, 2013]. Under certain conditions, as these linear contrails age, they spread and form contrail cirrus or aviation-induced cirrus [*Minnis et al.*, 1998; *Lee et al.*, 2009; *Schumann and Graf*, 2013]. *Minnis et al.* [2013] used satellite data and found that the mean optical depths and effective particle sizes of contrail cirrus were 2–3 times larger and 20% greater, respectively, than the corresponding values retrieved for the adjacent linear contrails. They also found that when contrails form below, in, or above existing cirrus clouds, the column cloud optical depth is increased and particle size is decreased even without increased cirrus coverage. Both linear contrails and contrail cirrus can warm the Earth due to their high altitudes and cold temperatures [*Lee et al.*, 2009]. Linear contrails are estimated to cause a global forcing of between 0.0057 and 0.011 W m^{-2} (a warming) [*Spangenberg et al.*, 2013; *Yi et al.*, 2012]. Linear contrails and contrail cirrus together have a larger global radiative forcing, estimated to range from 0.0375 W m^{-2} to 0.05 W m^{-2} [*Burkhardt and Kärcher*, 2011; *Schumann and Graf*, 2013]. *Gettelman and Chen* [2013] studied the aviation-induced cloudiness (similar to contrail cirrus) in a global climate model (GCM) model and showed a warming effect of 0.016 W m^{-2}.

The second aviation-induced effect on clouds is through the effect of aircraft-emitted particles (namely, those containing black carbon, sulfate, and organic compounds) acting as cloud condensation nuclei (CCN) and heterogeneous ice nuclei (IN) [*Kärcher et al.*, 2007]. If aircraft-emitted soot (soot = black carbon + organic matter) can act as heterogeneous ice nuclei (IN), they would require a lower relative humidity to nucleate than that required by homogeneous freezing. Therefore, if there are enough IN present, they may nucleate prior to any homogeneous nucleation and consume the available water vapor, thus inhibiting homogeneous freezing. Of course, the specific ability of a given particle to act as a heterogeneous nucleation

site depends on the local temperature, supersaturation, and its size. However, as summarized by *Kärcher et al*. [2007] (see their Table 4), the ice nucleating efficiency (defined as the fraction of particles that can act as potential IN) of soot acting as IN is subject to great uncertainties depending on the fuel type, its coating by sulfate, and many other factors. Nevertheless, this potential effect of aircraft soot as IN should not be ignored in global climate modeling, although assumptions of the specific ice nucleating efficiency of aircraft soot is generally needed.

Hendricks et al. [2005] first used a GCM to show that aircraft black carbon (BC) when acting as efficient IN could either decrease or increase the ice water path depending on whether the background ice nucleation was homogeneous or heterogeneous. *Penner et al*. [2009] also assumed that aircraft-emitted soot was efficient heterogeneous IN and first calculated its radiative impact on the large-scale cirrus clouds. They found a negative (cooling) radiative forcing ranging from -0.12 to $-0.16\,\mathrm{W\,m^{-2}}$ using an off-line global model with two different ice nucleation schemes. The net negative forcing was caused by the addition of IN to a background atmosphere (mainly in the tropics and southern hemisphere) that was dominated by homogeneous nucleation. Using a much smaller nucleating efficiency of 0.1% for the aviation black carbon (BC) as heterogeneous IN in cirrus clouds, *Gettelman and Chen* [2013] did not find a statistically significant effect from aviation BC in ice clouds. However, when they increased the aviation BC heterogeneous IN number by assuming a smaller size (11 nm) of BC as well as a larger nucleating efficiency of 2%, they were able to get a statistically significant effect of $-0.096\,\mathrm{W\,m^{-2}}$.

This study examines the sensitivity of climate forcing from the aircraft-emitted soot acting as IN to the background ice nucleation processes. Instead of assuming a fixed nucleating efficiency as in *Penner et al*. [2009] or *Gettelman and Chen* [2013], we follow the formation of persistent contrail cirrus clouds and assume that only the aircraft soot that has previously frozen within a contrail formed immediately after emission can act as good IN thereafter. As the climate impact from these aircraft soot IN is affected by the existing background heterogeneous IN as well as the haze droplet number, we will vary the background IN (dust in this study) number and the haze droplet (sulfate aerosol in this study) number to estimate the sensitivity of the forcing caused by aircraft soot IN. Models and experiments are described in section 2, results are presented in section 3, and conclusions and discussion are in section 4.

2. Model and Experiments

2.1. Description of the Coupled CAM5/IMPACT Model

We used the coupled Community Atmosphere Model version 5.2 (CAM5)/IMPACT model in this study. The CAM5/IMPACT model embeds the University of Michigan IMPACT aerosol model as a module in the Community Atmosphere Model version 5.2 (CAM5). CAM5 is the atmospheric component of the Community Earth System Model version 1.1. The IMPACT aerosol module simulates a total of 17 externally mixed aerosol types and/or size bins: 3 sizes representing the number and mass of pure sulfate aerosols (i.e., nucleation, Aitken, and accumulation modes), 3 types of fossil/biofuel soot that depend on its hygroscopicity or the amount of sulfate on the soot, 2 aircraft soot modes (preactivated in contrails or not), 1 biomass soot mode, 4 dust sizes, and 4 sea-salt sizes. All these aerosols may mix with sulfate through condensation and coagulation processes or through sulfate formation in cloud drops. Thus, for all nonsulfate aerosols, we also track the amount of sulfate mass coated on them. The performance of the off-line IMPACT model driven by CAM5 meteorological fields was previously evaluated by *Zhou et al*. [2012]. The overall characteristics of the performance of this new IMPACT module within CAM5 are similar to this off-line version. CAM5 also uses its own aerosol treatment, the 3 modal aerosol module (MAM3), which treats three externally mixed modes (i.e., Aitken, accumulation, and coarse modes). It assumes internal mixing of all major aerosol species (sulfate, black carbon, primary organic carbon, secondary organic carbon, mineral dust, and sea salt) within each mode and predicts the mass mixing ratio of different aerosol species in each mode but one summed number mixing ratio of each mode [*Liu et al*., 2012a]. In the current coupled model, both aerosol modules (IMPACT and MAM3) run in CAM5. Aerosols simulated by the IMPACT module do not interact with any physical processes except in cirrus clouds (below -35°C), which use sulfate and dust numbers from MAM3 and *additional* heterogeneous ice nuclei (IN) from the preactivated aircraft soot simulated by the IMPACT module. One of the advantages of using the IMPACT module to simulate the aircraft soot rather than adding it to the background soot in MAM3 is that the IMPACT module can track the aircraft soot as an

individual constituent so that we are able to use a different ice nucleating efficiency for aircraft soot as heterogeneous IN compared to that of the background soot.

2.2. CAM5 Ice Nucleation for Cirrus Clouds

The ice nucleation for cirrus clouds (below −35°C) in CAM5 follows *Liu and Penner* [2005] (hereafter the LP parameterization) and was implemented in CAM3 by *Liu et al*. [2007] and later in CAM5 by *Gettelman et al*. [2010]. The LP parameterization can treat the competition between homogeneous freezing on sulfate haze droplets and heterogeneous nucleation on dust (immersion freezing) as well as other potential heterogeneous IN like soot particles from both biomass burning and fossil fuel. The default setup of CAM5 assumes that homogeneous nucleation takes place only on Aitken mode sulfate aerosol particles with diameter larger than 0.1 μm, while heterogeneous nucleation only occurs on dust particles in the coarse mode (diameter larger than 1 μm) [*Gettelman et al*., 2010, 2012; *Gettelman and Chen*, 2013].

In contrast to the treatment of homogeneous nucleation in *Gettelman et al*. [2010], *Liu et al*. [2012a, 2012b] and *Zhang et al*. [2013] assumed that the total sulfate number in the Aitken mode participates in homogeneous nucleation rather than only a fraction of Aitken mode particles. Using the total sulfate number in the Aitken mode is more consistent with how the LP parameterization was initially developed because the total sulfate number rather than a portion of a lognormal mode was used initially in the parcel model to obtain the empirically fitted curves in LP [*Liu and Penner*, 2005]. As will be shown in Table 2 in section 3, the simulated radiative properties (i.e., short- and long-wave cloud forcings) at the top of atmosphere (TOA) are very sensitive to the number of sulfate particles used in the homogeneous freezing parameterization. In the current implementation of the LP parameterization in CAM5, the condensation of water vapor onto preexisting ice particles during the calculation of new ice particle formation is not included. Including water vapor condensation onto preexisting ice particles either prior to ice nucleation or during its formation could significantly decrease the number of ice particles formed [*Hendricks et al*., 2011; *Kuebbeler et al*., 2014]. Thus, it is possible that the frequency of ice nucleation occurrence treated in CAM5 for cirrus is too high, and the ice number from homogeneous freezing may be overestimated. In this paper, we used both the full Aitken sulfate number and the portion with $D > 0.1$ μm to examine the importance of these two homogeneous freezing assumptions for the calculation of aircraft soot forcing.

Another source of uncertainty lies in the treatment of the background heterogeneous IN. In the default CAM5 setup, only dust in the coarse mode is considered as heterogeneous IN [*Gettelman et al*., 2010]. However, *Liu et al*. [2012a, 2012b] and *Zhang et al*. [2013] used both coarse mode and accumulation mode. Theoretically, the effectiveness of dust acting as heterogeneous IN depends on the number of "active" sites present on its surface. Thus, both small and large dust particles could potentially serve as heterogeneous IN even though coarse mode dust may be more efficient due to its larger surface area [*Möhler et al*., 2006; *Welti et al*., 2009]. The ice nucleation efficiency of dust is generally less than 100% depending on the size as well as the type and its coating [*Möhler et al*., 2006, 2008; *Welti et al*., 2009]. In this study, we will follow the use of 100% ice nucleation efficiency of dust as in the standard CAM5 setup but varying the dust IN number by using only coarse mode dust as IN or using both coarse mode and accumulation mode dust as IN. We calculate the aircraft soot IN forcing under these two different scenarios. Recent studies by *Gettelman et al*. [2012] and *Gettelman and Chen* [2013] also included black carbon (BC) as an additional IN source in CAM5. Here, to simplify our study, we focus on treating only dust as heterogeneous IN without including background BC. In section 3, we also show that the use of dust from both coarse and accumulation modes gives higher IN numbers than suggested by the observations [*Rogers et al*., 1998] potentially due to the use of a higher than realistic ice nucleating efficiency

2.3. Aircraft Soot as Heterogeneous IN

While fresh aircraft soot may not nucleate ice particles at relative humidities below water saturation [*Koehler et al*., 2009], the behavior of soot that has been processed in contrails has not been measured. The preactivation of such soot may allow it to nucleate at lower relative humidities (or higher temperatures), and this is an important possibility to consider. We note that a large number of organic substances have been shown to freeze at higher temperatures than the temperature required when they first freeze [*Evans*, 1967]. *Edwards et al*. [1970] showed that preactivation occurs with a variety of organics by "ordering" of ice monolayer left on surface of particle. *Wagner et al*. [2012] found ice-processed organics freeze at

Table 1. Summary of Experiments and Main Results

Case[a]	Assumed Sulfate Solution Number or IN[b]	Main Results
$H_{sulf}L_{dust}$	Homogeneous freezing on high sulfate number, heterogeneous nucleation on low dust number	Net global cooling, $-0.35\,W\,m^{-2}$
$H_{sulf}H_{dust}$	Homogeneous freezing on high sulfate number, heterogeneous nucleation on high dust number	Net global cooling, $-0.29\,W\,m^{-2}$
$L_{sulf}L_{dust}$	Homogeneous freezing on low sulfate number, heterogeneous nucleation on low dust number	Net global warming, $0.09\,W\,m^{-2}$
$L_{sulf}H_{dust}$	Homogeneous freezing on low sulfate number, heterogeneous nucleation on high dust number	Net global warming, $0.09\,W\,m^{-2}$
Het_H_{dust}	Heterogeneous nucleation only, on high dust number	Net global warming, $0.11\,W\,m^{-2}$
Het_L_{dust}	Heterogeneous nucleation only, on low dust number	Net global warming, $0.21\,W\,m^{-2}$

[a]Each case includes two simulations: the base one without aircraft emissions and the one with aircraft emissions.
[b]High sulfate number is the total sulfate number in the Aitken mode, low sulfate number is the number of sulfate with diameter $> 0.1\,\mu m$ in Aitken mode, high dust number is the number of dust from both accumulation and coarse modes, and low dust number is the number dust from coarse mode only.

supersaturations (with respect to ice) from 5 to 30% (well below their homogeneous freezing limit which occurs if the particles are cooled starting a few degrees below glass transition). *Adler et al*. [2013] found that ice-processed organic particles have a porous structure due to phase separation upon freezing, subsequent glass transition, and ice sublimation. Such modified aerosols can be better ice and cloud condensation nuclei and scatterless light.

Different nucleating efficiencies have been assumed in the literature (100% by *Hendricks et al*. [2005], 100% by *Penner et al*. [2009], and 0.1% and 2% by *Gettelman and Chen* [2013]). Here, instead of assuming a fixed fraction, we follow the formation of persistent contrail cirrus in this study and assume that only aircraft soot that has been previously frozen in contrail cirrus is "preactivated" and becomes good IN thereafter.

We used hourly global aircraft soot emissions for 2006 from the Aviation Environment Design Tool data set [*Barrett et al*., 2010] in the IMPACT module, which predicts two types of aircraft soot, preactivated and "inactive" aircraft soots. We used a lognormal size distribution with a geometric standard deviation of 1.6 and a geometric diameter of 60 nm to calculate the initial aircraft soot number [*Barrett et al*., 2010]. Emission of aircraft soot is put into the preactivated type when the ambient temperature and relative humidity satisfy the following three criteria:

1. the ambient temperature is below a critical temperature, T_c (see below);
2. the ambient relative humidity is higher than a critical relative humidity, RH_c; and
3. the ambient relative humidity over ice is greater than 100%.

The first two criteria are the Schmidt–Appleman criterion for the formation of contrails [*Schmidt*, 1941; *Appleman*, 1953; *Schumann*, 1996], and the third one is required for persistent contrail cirrus to form. This latter criterion may lead to an underestimate of the number of soot particles that may have been incorporated within contrails but is a conservative number. The calculations of the critical temperature T_c and critical relative humidity RH_c follow *Chen et al*. [2012] and are presented in the supporting information. Preactivated aircraft soots remain good ice nuclei until there are three or more monolayers of sulfate coated on the surface of soot, and then it is removed from the preactivated type and put into the inactive type. This treatment follows findings by *Koehler et al*. [2009] and *Cziczo et al*. [2009], which showed that an increase in the hygroscopicity of particles causes a decrease in the nucleating efficiency. In section 3.3, we will show that the preactivated aircraft soot only accounts for ~0.6% of the total aircraft soot in the air.

2.4. Experiment Description

Table 1 describes the experimental setup for background aerosol acting as ice nuclei. Each experiment includes two simulations, one with aircraft soot as extra heterogeneous IN and one without. All simulations have a horizontal resolution of 1.9°×2.5° and are run for 21 years. We analyze the last 20 years, which provide robust global statistics.

The first four cases in Table 1, $H_{sulf}L_{dust}$, $H_{sulf}H_{dust}$, $L_{sulf}L_{dust}$, and $L_{sulf}H_{dust}$, use different combinations of sulfate and dust number concentrations for the background homogeneous freezing and heterogeneous

nucleation, respectively. High sulfate numbers assume that the total Aitken mode sulfate concentration contributes to ice freezing, while low sulfate numbers include only sulfate concentrations with diameter larger than 0.1 μm. High dust numbers include both the accumulation and coarse modes. Low dust numbers include only the coarse mode. As will be shown in section 3, a net radiative cooling effect at the top of the atmosphere occurs when the background homogeneous freezing is inhibited by the aircraft soot IN. As we show below, the tropical Indian Ocean, Southeast Asia, and Central America are among the main regions with background freezing dominated by homogeneous freezing and thus are the largest contributing regions to the net cooling effect from aircraft soot IN. However, recent studies by *Jensen et al*. [2013] and *Cziczo et al*. [2013] used in situ observations to argue that heterogeneous nucleation may be the predominant ice nucleation process in cirrus near the tropical tropopause layer and at altitudes varying from 5 km to 16 km. Therefore, to explore the possible consequences of tropical regions dominated by heterogeneous ice nucleation, we also include two pure heterogeneous cases, Het_H_{dust} and Het_L_{dust}. By excluding homogeneous freezing, we eliminate any strong net cooling effect in tropical regions. We expect that these two cases will result in a net warming effect from the aircraft soot, which should be considered as upper limits.

To determine which background freezing case (i.e., base case) is most relevant, we compared the in-cloud ice crystal numbers from each simulation with observations. However, as will be shown in section 3, the comparison failed to differentiate a "best" case. More details of the comparison are presented in section 3. As the graphical differences between the results from the cases $H_{sulf}L_{dust}$ and $H_{sulf}H_{dust}$ and between $L_{sulf}L_{dust}$ and $L_{sulf}H_{dust}$ are much smaller than the differences from other cases, we only present graphs from one of each pair.

3. Results

Figure 1 shows the simulated emissions, burden, and zonally averaged number of preactivated aircraft soot from case $L_{sulf}L_{dust}$, the case that has been set up similar to the default CAM5 case. The annual emission that meets the three criteria listed in section 2.2 for persistent contrail cirrus is 9.28×10^5 kg/yr, which is ~8% of the total aircraft soot emission. Major emission regions include North America, North Atlantic Ocean, Europe, and East and Southeast Asia. As the majority of the aircraft soot is directly emitted to the upper troposphere and the lower stratosphere (UTLS), where it is subject to less wet deposition, the overall lifetime of the total aircraft soot (preactivated and inactive) is ~33 days, much longer than that of other aerosols simulated in the IMPACT module which are typically on order of 1 week or less [*Zhou et al*., 2012]. However, since we assume that the preactivated soot can lose its ability to act as IN when there are three or more monolayers of sulfate coated on it, the preactivated soot has a much shorter lifetime of ~2.6 days and a much smaller burden, 6.54×10^3 kg, which represents only ~0.6% of the total aircraft soot loading. The annually and zonally averaged number concentrations of the preactivated aircraft soot in the UTLS region of the northern hemisphere (NH) is about 0.01 cm^{-3} to 0.1 cm^{-3}. The soot number in the UTLS region of the southern hemisphere (SH) is smaller by 1 order of magnitude but not negligible, about 0.001 cm^{-3} to 0.01 cm^{-3}. Although most flight activities are in the NH, there are still some flights in the SH. Advection can also play a role in transporting aircraft soot from the tropics toward the South Pole. Results from the other five cases in Table 1 show similar emissions, burdens, and lifetimes for aircraft soot.

Figure 2 shows the annual mean high and low sulfate/dust numbers as well as the preactivated aircraft soot IN numbers at ~233 hPa, which is the main flight level. The results of high sulfate and dust numbers are taken from case $H_{sulf}H_{dust}$, while the other results are taken from case $L_{sulf}L_{dust}$. Note that the color bar in Figure 2a has a different scale. The sulfate number from the entire Aitken mode shown in Figure 2a is on the order of 100 cm^{-3}, while the number of sulfate particles with diameter larger than 0.1 μm shown in Figure 2c is about 2 orders of magnitude smaller, roughly on the order of 1 cm^{-3}. As shown in Figure 2b, in most areas in the NH, the dust number from the sum of the accumulation and coarse modes ranges from 0.1 to 0.3 cm^{-3}. For the low dust number case (dust from only the coarse mode) shown in Figure 2d, the number concentration ranges from 0.01 to 0.05 cm^{-3} near the major source regions and downwind. Near the source regions (e.g., North Africa and Arabian Peninsula) and the downwind area (e.g., central Atlantic Ocean), the dust number from the sum of the accumulation and coarse modes (Figure 2b) is about 3 to 4 times larger than that from only the coarse mode (Figure 2d). However, in the remote areas (e.g., the two polar regions), the difference can be as large as a factor of 20 due to the faster removal of the coarse

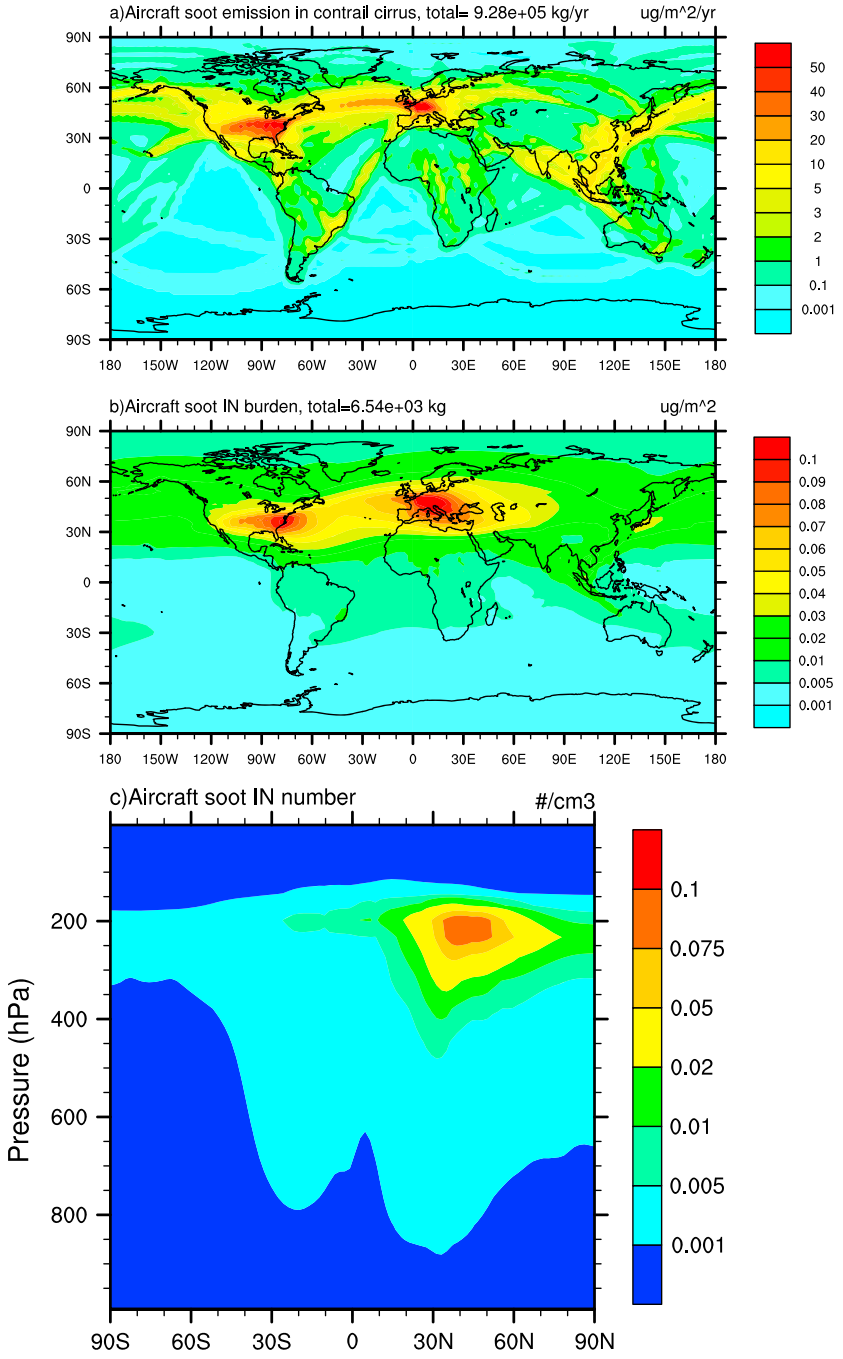

Figure 1. (a) Vertically integrated emission of aircraft soot that forms persistent contrail cirrus. (b) Column-integrated burden of aircraft soot IN. (c) Annual and zonally averaged aircraft soot IN numbers. All results are from case $L_{sulf}L_{dust}$.

mode dust through gravitational settling. According to the estimate from *Hendricks et al.* [2005], which was based on the in situ observational results of *Rogers et al.* [1998], IN concentrations larger than 0.5 cm^{-3} are comparatively rare in the UTLS (~60% of the measured IN concentrations are smaller than 0.01 cm^{-3}, and ~95% are smaller than 0.1 cm^{-3}). Using the dust number from both accumulation mode and coarse mode in Figure 2b may overestimate the IN number, while using the dust number from the coarse mode only in Figure 2d may underestimate the IN number. The simulated preactivated aircraft soot IN number in Figure 2e ranges from 0.1 to 0.3 cm^{-3} in North America and Europe and is larger than 0.01 cm^{-3} everywhere in the middle to high latitudes in the NH. It is about the same magnitude or slightly larger (by a factor of ~2)

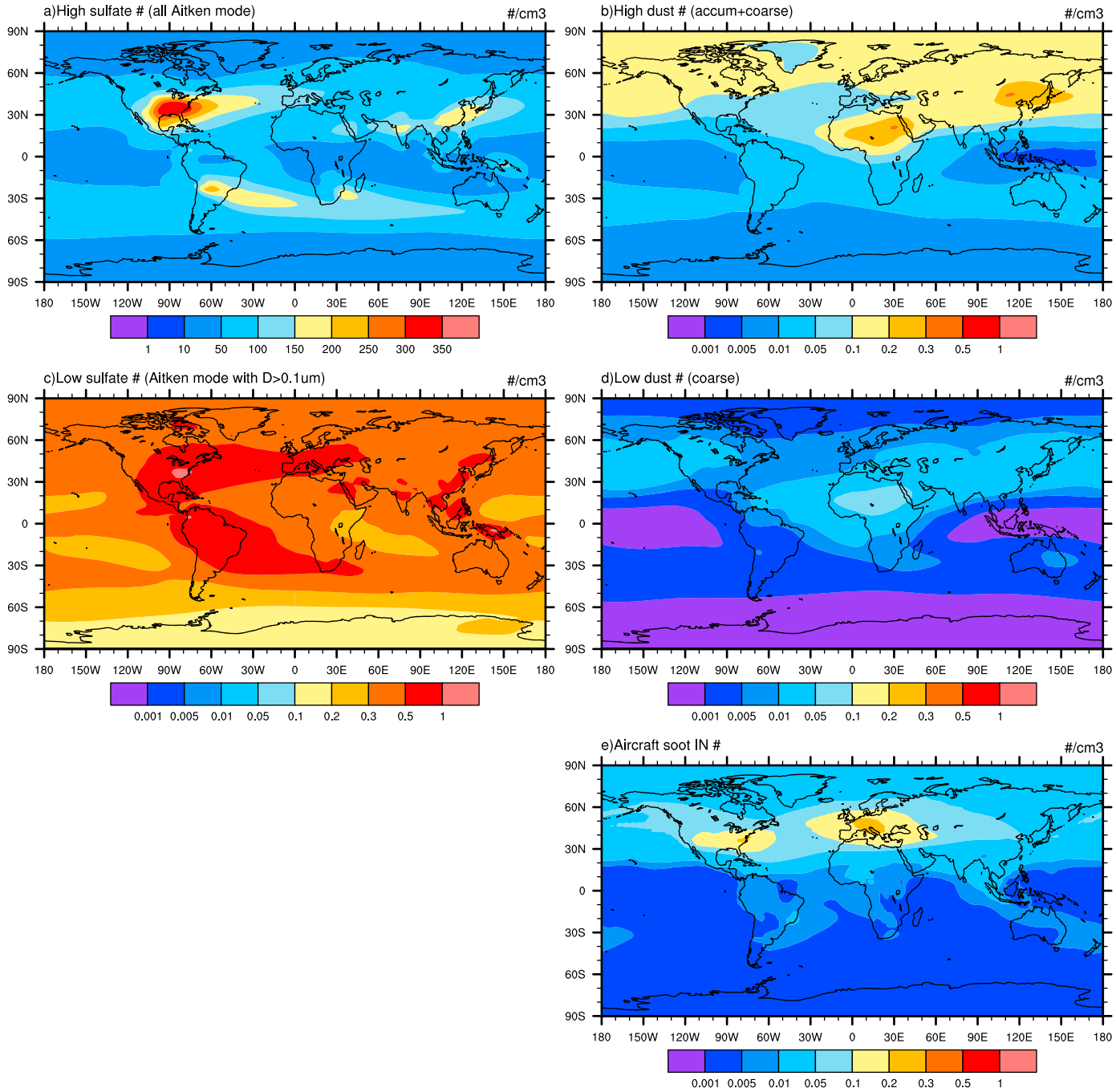

Figure 2. Sulfate, dust, and aircraft soot IN numbers at ~233 hPa. (a) Sulfate number in the Aitken mode used to calculate homogeneous nucleation in case $H_{sulf}H_{dust}$. (b) Dust numbers from both accumulation mode and coarse mode used to calculate heterogeneous nucleation in case $H_{sulf}H_{dust}$. (c) Sulfate number in the Aitken mode with diameter $>$ 0.1 μm used to calculate homogeneous nucleation in case $L_{sulf}L_{dust}$. (d) Dust number in the coarse mode used to calculate heterogeneous nucleation in case $L_{sulf}L_{dust}$. (d) Aircraft soot IN number from case $L_{sulf}L_{dust}$.

than that from the high dust number in Figure 2b in North America and Europe. It is worth noting that even though the aircraft soot in Southeast Asia is smaller than that in the U.S. and Europe, it is about 2 times larger than the high dust number in this area. This is due to the strong wet removal by the convective precipitation, which causes an extremely low dust number at this altitude and a background that is dominated by homogeneous freezing. We show below that Southeast Asia and its downwind region, the tropical Indian Ocean, are the major areas where the aircraft soot could have a huge impact due to the high

Table 2. Key Cloud Properties for Cases Without Aircraft Soot

	SWCF[a] (W m^{-2})	LWCF (W m^{-2})	IWP (g m^{-2})	LWP (g m^{-2})
Observation[b]	−47.1	26.5		
$H_{sulf}L_{dust}$	−61.1	33.5	21.4	47.5
$H_{sulf}H_{dust}$	−60.2	32.6	20.9	47.0
$L_{sulf}L_{dust}$	−52.1	24.1	17.7	44.6
$L_{sulf}H_{dust}$	−52.8	25.0	18.1	45.0
Het_L_{dust}	−49.5	20.4	15.7	44.0
Het_H_{dust}	−51.1	23.0	17.1	44.5

[a]SWCF: short-wave cloud forcing, LWCF: long-wave cloud forcing, IWP: ice water path, and LWP: liquid water path.
[b]From the updated version 2.1 of the Clouds and the Earth's Radiant Energy System-Energy Balanced and Filled data described by Loeb et al. [2009]; see Table 2 of *Gettelman et al*. [2012].

aircraft soot IN to dust IN ratio. In the rest of the world, the aircraft soot number is at least 4 times smaller than the dust number for the high dust case. Compared to the dust number in the low dust case (Figure 2d), the aircraft soot IN number is about 1 order of magnitude larger in North America, Europe, and Southeast Asia and about the same magnitude as the dust number for this case in the rest of the world. Including the aircraft soot as IN in the $L_{sulf}L_{dust}$ case allows the modeled IN to compare better with the observed IN from *Rogers et al*. [1998].

Table 2 gives the global and annual mean short-wave cloud forcing (SWCF), long-wave cloud forcing (LWCF), ice water path (IWP), and liquid water path (LWP) from the base cases without aircraft soot emissions. The SW and LW cloud forcings as well as the IWP are most sensitive to the sulfate numbers and less sensitive to the dust numbers. Case $H_{sulf}L_{dust}$, which uses the high sulfate number for homogeneous freezing and low dust number for heterogeneous nucleation, gives the largest SWCF, LWCF, IWP, and LWP due to the high ice crystal number concentrations simulated from the homogeneous freezing. Using the low sulfate number while keeping the dust number the same dramatically decreases both SWCF (less cooling) and LWCF (less warming) by ~7–9 W m^{-2} in cases $L_{sulf}L_{dust}$ and $L_{sulf}H_{dust}$. These large deceases in cloud forcings come from decreases in both IWP and LWP. For example, the IWP decreases from 20.9 g m^{-2} in case $H_{sulf}H_{dust}$ to 17.7 g m^{-2} in case $L_{sulf}L_{dust}$, while the LWP decreases from 47.0 g m^{-2} to 44.6 g m^{-2}. The decrease in IWP is due to the change in ice number concentration, while the decrease in LWP is caused by dynamical feedback. Thus, in the two low sulfate number cases, the low sulfate number, especially in the upper tropical troposphere, leads to fewer but larger ice particles, which lead to a larger gravitational removal of ice. Less ice in the upper troposphere reduces the local heating rates and causes a cooler upper troposphere and more convection. The enhanced convection leads to more convective precipitation, which reduces the delivery of water vapor to the upper troposphere as well as the total precipitable water vapor. The total precipitable water may also decrease due to the enhanced convective precipitation in the tropics. This decrease then causes smaller LWP and less precipitation from large-scale clouds. The two pure heterogeneous cases, Het_H_{dust} and Het_L_{dust}, give the smallest cloud forcings, IWP, and LWP. Increasing the dust number from case $H_{sulf}L_{dust}$ to case $H_{sulf}H_{dust}$ decreases IWP, and thus, the magnitude of the cloud forcings as some homogeneous freezing (mainly in the NH) is inhibited by the extra dust IN. While increasing the dust number from $L_{sulf}L_{dust}$ to $L_{sulf}H_{dust}$ can also increase the inhibition of some homogeneous freezing, the increases of IWP in the middle latitudes of NH, where heterogeneous nucleation already dominates, outweigh the loss of IWP in other places thereby producing a small increase in IWP.

3.1. Impact on Ice Nucleation

Figure 3 shows the ratio of newly activated ice crystals produced by homogeneous freezing with and without aircraft soot as extra IN to the total newly activated ice crystals produced from both homogeneous and heterogeneous freezing. As shown in Figure 3a, without the aircraft soot IN, the fraction of homogeneous freezing near 200–300 hPa from the $H_{sulf}H_{dust}$ base case is more than 90% in the SH and the tropics and is about 40%–80% at the middle to high latitudes in the NH. Adding extra aircraft soot IN reduces these fractions in both hemispheres (Figure 3b). The difference in the fraction of homogeneous freezing with and without aircraft soot is shown in Figure 3c. The largest decrease occurs at the middle latitudes in the NH, where the aircraft soot emissions are largest. In the tropics, the largest changes occur around ~250 hPa with decreases above that altitude. In Figure 1c, we see that the highest aircraft soot IN number is centered

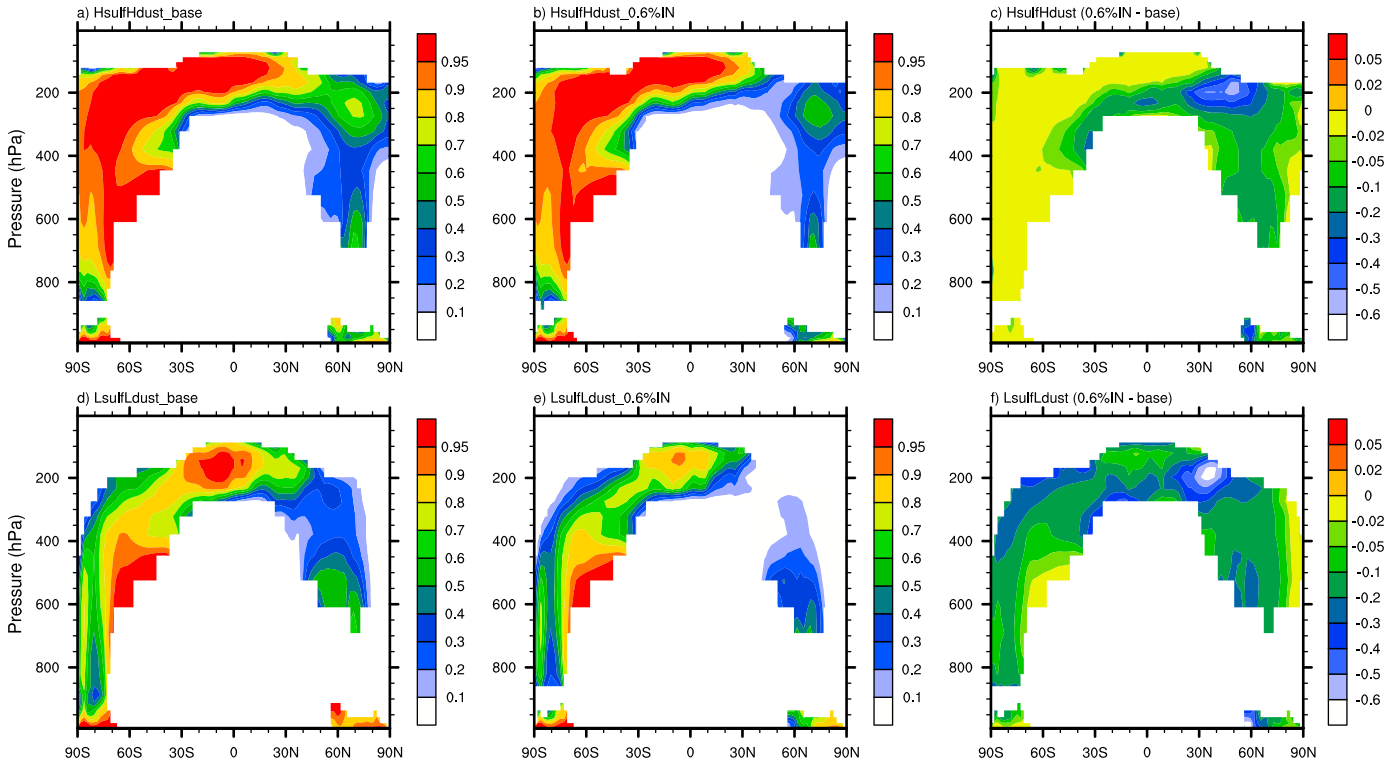

Figure 3. Fractions of annually and zonally averaged newly activated ice crystals from homogeneous freezing from (left column) the base cases without aircraft emissions, (middle column) cases with ~0.6% of aircraft soot as IN, and (right column) the differences. The top graphs are from the $H_{sulf}H_{dust}$ cases, and the bottom graphs are from the $L_{sulf}L_{dust}$ cases.

about 200 hPa in the tropics. This difference in the peak heights between the emission of soot and the IN effect on ice nucleation can be explained by the required heterogeneous IN number to suppress homogeneous freezing in the LP parameterization for ice clouds, since the required IN number increases as the temperature decreases. Therefore, the inhibition of homogeneous freezing is more likely to occur near ~250 hPa, where the temperature is higher despite the fact that the aircraft soot IN concentration is relatively lower at this altitude compared to higher levels. The change in the southern hemisphere is smaller since the aircraft soot IN number is significantly smaller here than in the NH. In addition, the ice number formed from the homogeneous freezing is much larger than that from the heterogeneous freezing so that the contribution of newly formed ice from homogeneous freezing still dominates even when its occurrence frequency decreases. For the $L_{sulf}L_{dust}$ base case (see Figure 3d), the fraction of homogeneous freezing is smaller almost everywhere than that from the $H_{sulf}H_{dust}$ base case in Figure 3a. Fractions over 90% are largely confined to the tropics (see Figure 3d), because the background IN are quickly removed through wet deposition processes in this region. At the middle to high latitudes in the NH, the fraction of newly formed ice from homogeneous freezing is close to 30% or less, significantly smaller than the fraction in the $H_{sulf}H_{dust}$ base case in Figure 3a. This relatively smaller fraction in the $L_{sulf}L_{dust}$ case is caused by the use of a much smaller sulfate number (~2 orders smaller in magnitude) than that used in the $H_{sulf}H_{dust}$ base case in the homogeneous freezing parameterization. Consequently, the contribution of the newly formed ice particles from homogeneous freezing is strongly reduced even though the actual occurrence frequency of the homogeneous freezing increases due to the smaller dust IN number used in the $L_{sulf}L_{dust}$ base case (not shown). Adding aircraft soot IN reduces the fraction to 10% or less at the middle to high latitudes in the UTLS region in the NH, where the majority of flight activities take place (see Figure 3e). Figure 3f shows the difference in the fraction of homogeneous freezing. The decrease in the tropics and SH is larger than that in Figure 3c.

Figure 4 shows the geographic distributions of the newly activated ice crystals produced through homogeneous freezing within the main flight level at ~233 hPa before and after adding aircraft soot IN. In

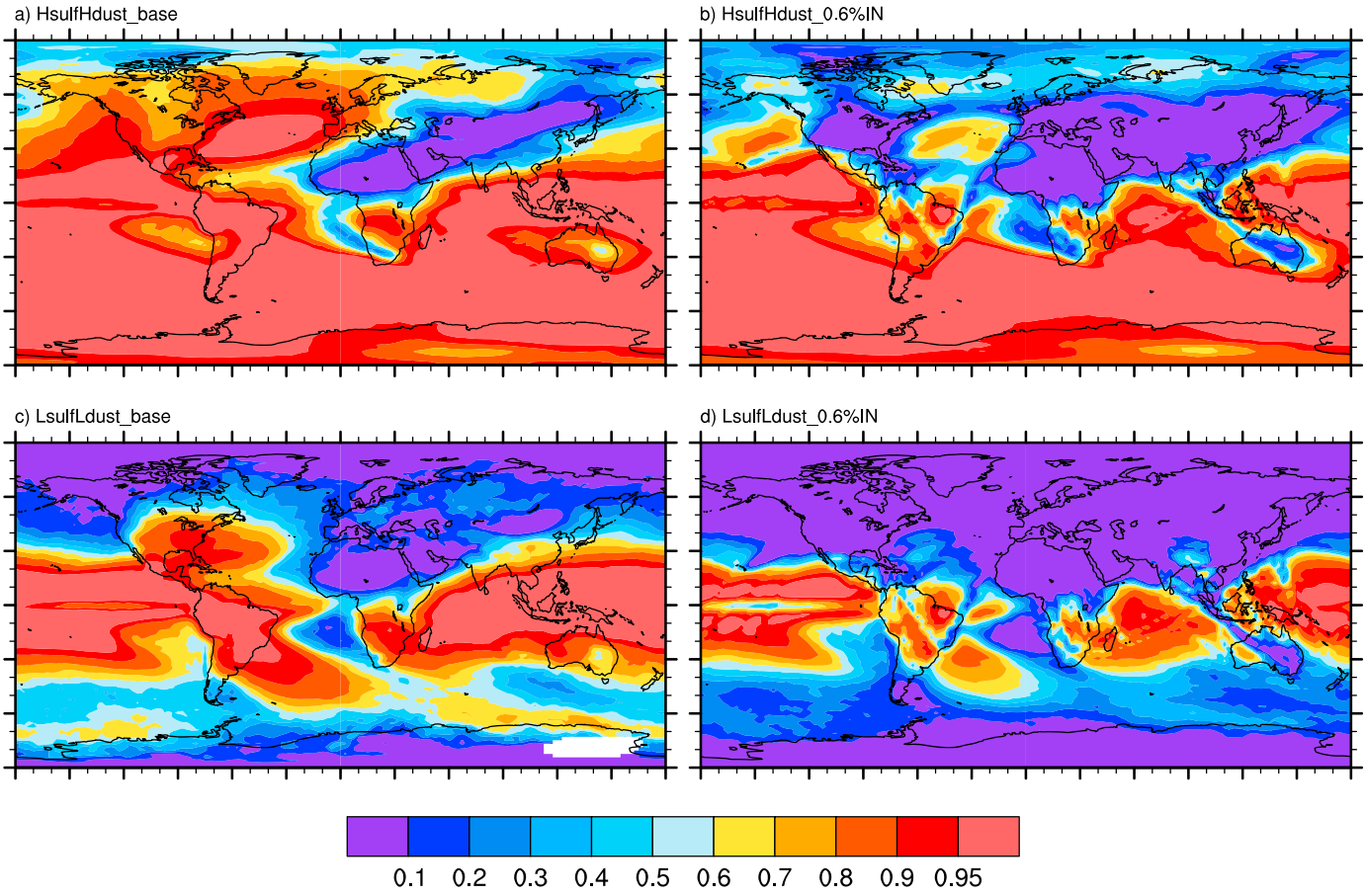

Figure 4. Fractions of annually averaged newly activated ice crystals from homogeneous freezing at ~233 hPa from (left column) the base cases and (right column) the cases with ~0.6% of aircraft soot as IN. The top graphs are from the $H_{sulf}H_{dust}$ cases, and the bottom graphs are from the $L_{sulf}L_{dust}$ cases.

the $H_{sulf}H_{dust}$ base case, the fraction is over 90% almost everywhere except in the major dust source regions in North Africa and Central Asia and downwind from these regions. The Arctic region also has lower fractions, since the dust number is high enough to compete with homogeneous freezing here. The regions with a homogeneous freezing fraction less than 10% expand and cover the U.S., Europe, and the other major flight routes (e.g., cross-Arctic routes, Europe to Africa routes, and Asia to Australia routes) after adding aircraft soot as IN. In the $L_{sulf}L_{dust}$ base case, the area dominated by heterogeneous freezing (i.e., with homogeneous freezing fraction less than 10%) is much larger (compare Figures 4c and 4a). After adding extra aircraft soot IN, the areas dominated by homogeneous freezing are limited to the tropical oceans and some regions over South America, where convective precipitation is able to efficiently remove heterogeneous IN (Figure 4d). In both base cases, we see that after adding aircraft soot IN, homogeneous freezing is almost entirely suppressed over the U.S. We note that *Zhang et al*. [2013] compared the modeled ice numbers to in situ-observed ice numbers from campaigns over the Southern Great Plains ARM site and suggested that homogeneous freezing is required to explain the observed increase in ice particle numbers with decreased temperature. So it is possible that the aircraft soot IN number used in this study is too high and that homogeneous freezing is suppressed too much. However, it is also possible that homogeneous freezing is suppressed too easily in the current CAM5 model parameterization. As mentioned earlier, the required heterogeneous IN number to suppress homogeneous freezing increases with decreased temperature in the LP parameterization. It also increases with the updraft velocity. CAM5 uses a single updraft velocity to determine the prevalence of homogeneous versus heterogeneous freezing and assumes an artificial maximum updraft velocity of 0.2 m s^{-1} in the LP parameterization. Such an assumption likely underestimates the prevalence of homogeneous freezing as this 0.2 m s^{-1} upper limit is reached most of the time in the upper troposphere [*Liu et al*., 2012b]. *Zhang et al*. [2013] suggested that this artificial

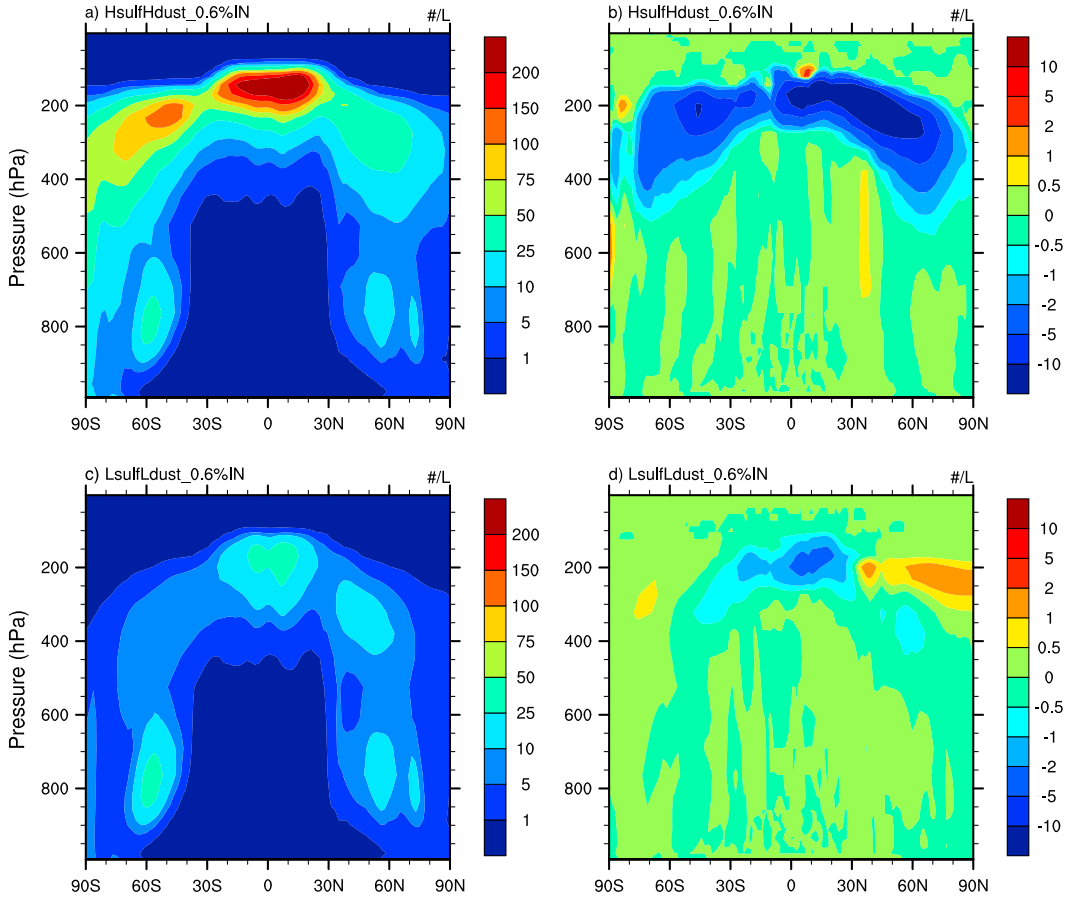

Figure 5. (left) Annually and zonally averaged ice crystal number concentrations (/L) from the base cases and (right) the change in number concentration after adding ~0.6% of aircraft soot as IN. The top graphs are from the $H_{sulf}H_{dust}$ cases, and the bottom graphs are from the $L_{sulf}L_{dust}$ cases.

upper bound of 0.2 m s^{-1} is smaller by a factor of 1.5–2 than the average updraft velocity from multiple field campaign observations in this area, and this upper bound is also too low compared to the Interhemispheric Differences in Cirrus Properties from Anthropogenic Emissions observations [*Kärcher and Ström*, 2003]. Updraft velocities as large as 0.3–0.5 m s^{-1} have also been observed in tropic anvil cirrus [*Jensen et al.*, 2009]. For the same temperature, the required heterogeneous IN to suppress homogeneous freezing can double when the updraft velocity increases from 0.2 m s^{-1} to 0.3 m s^{-1}. Thus, we conclude that there is a model inhibition of homogeneous freezing that is larger than observations due to the model bias in updraft velocity rather than the treatment of aircraft soot as IN. To test the effects of this assumption, we increased the upper limit to 0.3 m s^{-1} and reran cases $H_{sulf}H_{dust}$ and $L_{sulf}L_{dust}$ for 10 years. In this sensitivity test, we see that after adding aircraft soot IN, there is still more than half of the continental U.S. with homogeneous nucleation fractions ranging from ~10% to ~90% in case $H_{sulf}H_{dust}$ and from ~10% to ~40% in case $L_{sulf}L_{dust}$ (see Figure S2 in the supporting information).

Figure 5 shows the annually and zonally averaged ice number concentrations and the change in ice number concentration after adding aircraft soot IN. The zonal mean ice number ranges from 10/L to 200/L in the $H_{sulf}H_{dust}$ base case and is largest in the tropics. The addition of aircraft soot IN decreases the ice number concentration almost everywhere by ~1/L to 20/L. The largest decrease appears at the middle latitudes in the NH and is consistent with the aircraft soot IN concentration in Figure 1c. However, the decrease in the SH is comparable to that in the NH, varying from about 1/L to 10/L, even though the aircraft soot IN number is roughly 1 order of magnitude smaller in the SH. This is because the SH is much more pristine (in terms of the concentration of heterogeneous IN in the background atmosphere) and dominated by homogeneous freezing in the base case as shown in Figure 3a. Thus, it only takes a small amount of extra

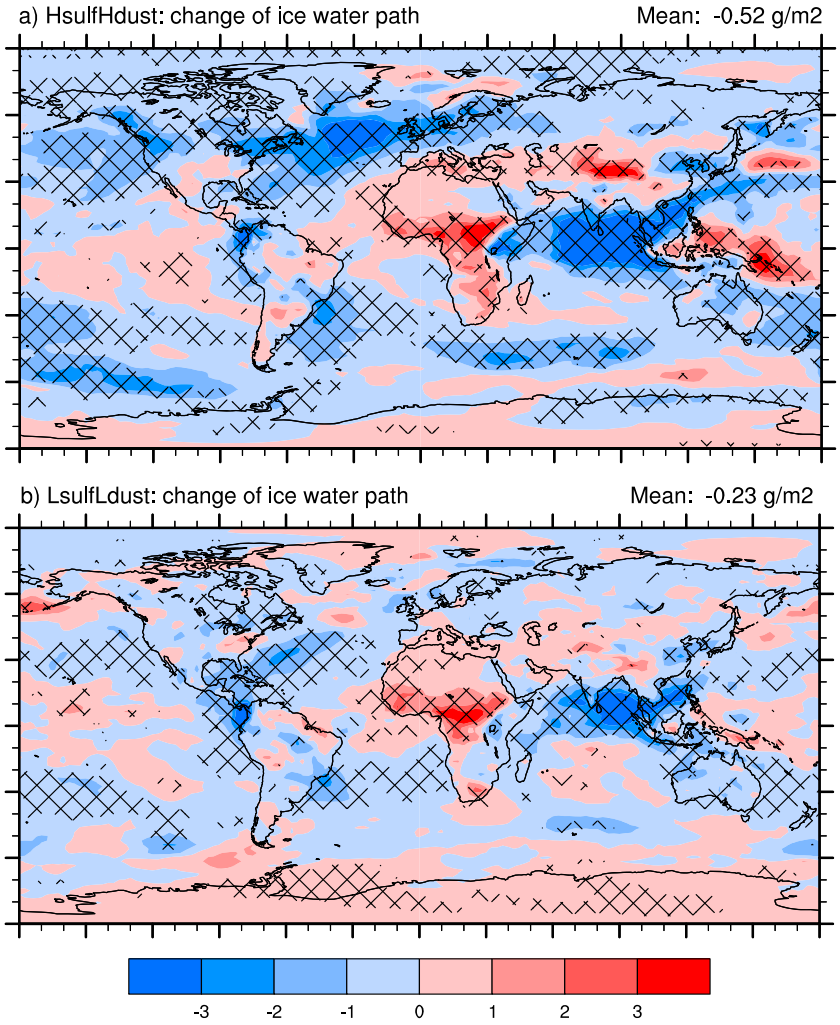

Figure 6. Changes in the annual mean ice water path after adding ~0.6% of aircraft soot as IN from (top) the $H_{sulf}H_{dust}$ case and (bottom) the $L_{sulf}L_{dust}$ case. Differences significant at the 90% level of the Student's *t* test are depicted by meshes.

aircraft soot IN to suppress some homogeneous freezing and cause a large decrease in ice number. The $L_{sulf}L_{dust}$ base case in Figure 4c has a much smaller zonal mean ice number, about 5/L to 50/L. This is because the ice number from homogeneous freezing is much smaller than that in the $H_{sulf}H_{dust}$ base case, since only a small portion (~1%) of the sulfate number in the Aitken mode is used in the LP ice nucleation parameterization (Figure 2c). Aircraft soot IN decrease the ice number in the tropics but increase it by ~0.5 L to ~2/L around 200 hPa from middle latitudes to the North Pole in the NH, where the heterogeneous freezing already dominates homogeneous freezing in the $L_{sulf}L_{dust}$ base case.

As we can see from the above discussion, the addition of aircraft soot IN can change the ice number significantly. However, we have not yet determined which case might best describe what occurs within the atmosphere. As this is critical to the radiative forcing, which we calculate in the next section, we compared the in-cloud ice crystal number concentration from each simulation with observations [*Krämer et al*. 2009]. Unfortunately, none of the cases described here is able to fully capture the trends in the observed ice crystal number concentrations (see Figure S1 in the supporting information). In all four cases with combined homogeneous and heterogeneous freezing, the in-cloud ice crystal number concentration decreases with increasing temperature, while the observation shows higher ice crystal number concentration in the temperature range from 205 K to 230 K than that in the temperature range from 190 K to 205 K. The two pure heterogeneous freezing cases show better agreement in the lower temperature range from 190 K to 205 K but underestimate in the higher temperature range from 205 K to 230 K. Adding extra aircraft

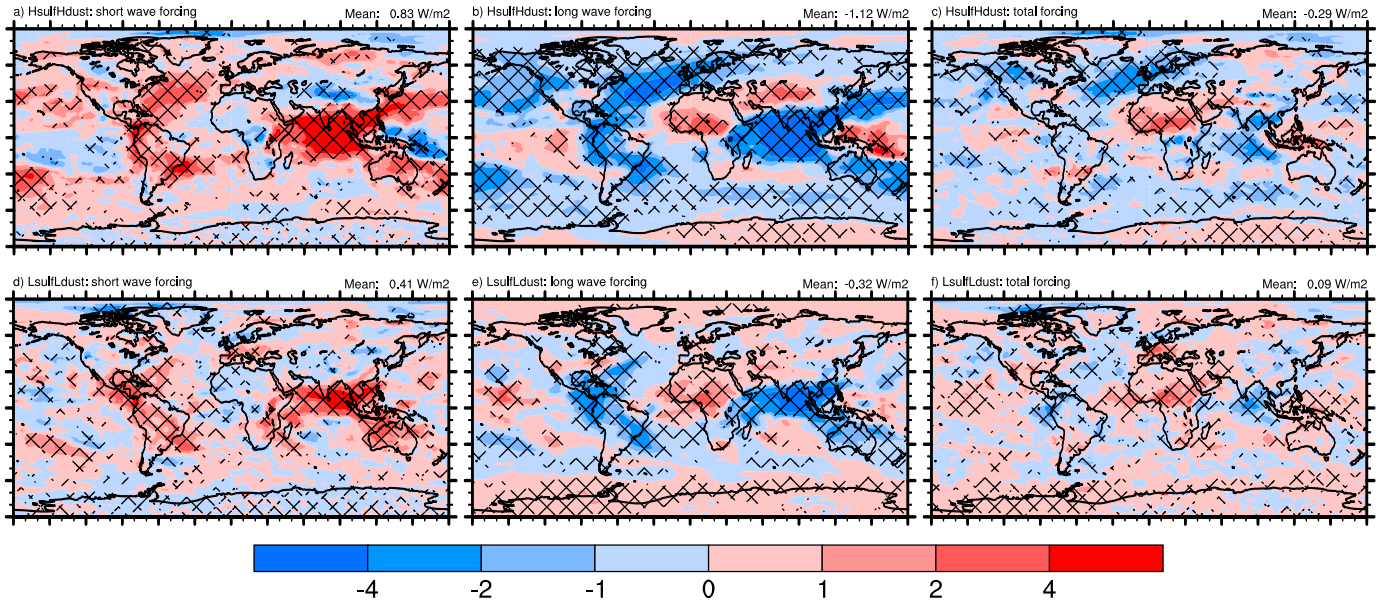

Figure 7. (left column) Annual mean all-sky short-wave radiative forcings, (middle column) long-wave radiative forcings, and (right column) total radiative forcings at the top of the atmosphere after adding ~0.6% of aircraft soot as IN. The top graphs are from the $H_{sulf}H_{dust}$ cases, and the bottom graphs are from the $L_{sulf}L_{dust}$ cases. Differences significant at the 90% level of the Student's *t* test are depicted by meshes.

soot IN slightly improves the comparison in case $H_{sulf}L_{dust}$ and $H_{sulf}H_{dust}$ by reducing the ice crystal number concentration simulated in the temperature range from 205 K to 230 K. But the opposite tendency with T is still present. Adding extra aircraft soot IN also improves the ice crystal number concentration in this temperature range in case Het_L_{dust} and Het_H_{dust}.

3.2. Radiative Forcing

Figure 6 shows the changes of ice water path (IWP) from the addition of aircraft soot for the $H_{sulf}H_{dust}$ and $L_{sulf}L_{dust}$ cases. In both cases, we see decreases of IWP over North America, Central America, North Atlantic Ocean, Europe, and the Indian Ocean, where the extra IN from aircraft soot decreases ice number by inhibiting some or all homogeneous freezing. As gravitational settling is the major removal mechanism for the ice particles, smaller ice number concentrations lead to larger ice particle sizes and faster removal. In North Africa, the Middle East, and Central Asia, where heterogeneous freezing is dominant due to high dust numbers (see Figure 3), ice number concentrations increase when heterogeneous IN from aircraft soot are added and thus the IWP increases. In Europe and near 60°S over the oceans in the SH, the $H_{sulf}H_{dust}$ case shows an obvious decrease of IWP. The decrease is smaller in these regions in the $L_{sulf}L_{dust}$ case.

Figure 7 shows the change in the all-sky short-wave radiative forcing, long-wave radiative forcing, and the total radiative forcing at the top of the atmosphere. The changes in the short-wave and long-wave radiative fluxes follow the changes of IWP and have opposite signs. The geographic pattern of the total radiative forcing (long-wave + short-wave) is similar to the pattern of the long-wave radiative forcing but of reduced magnitude. Some similarities can be observed in both cases: major areas with cooling include Central America, the North Atlantic Ocean, and the tropical Indian Ocean and major areas with warming include North Africa and western to central Asia. The background atmosphere in the major cooling areas is dominated by homogeneous freezing before adding aircraft soot IN as a result of the low dust numbers in these areas, while the background atmosphere is dominated by heterogeneous freezing in areas with a net warming. Statistics from 20 year simulations show that the forcings in these major cooling and warming areas pass the Student's *t* test for significance with a confidence level of 95%. Over the western Pacific Ocean warm pool region, there is a net warming which is consistent with the increased IWP shown in Figure 6. However, since the background heterogeneous IN are very low in this region, the added aircraft soot IN act to decrease the homogeneous freezing as shown in Figure 4. Therefore, this increased IWP and the associated warming effect at the TOA is not explained by the cloud microphysics, which should have caused a

decrease of the ice number as well as the IWP. Here we offer a possible explanation through the changes in the large-scale dynamics. We found a decrease in the large-scale updraft velocity in the upper troposphere over the tropical Indian Ocean and an increase over the western Pacific Ocean. The decrease in the large-scale ascending motion in the upper troposphere over the tropical Indian Ocean is related to the strong cooling effect due to the decreased ice water path caused by the added aircraft soot IN. This decreased large-scale ascent rate in the upper troposphere over the tropical Indian Ocean would be expected to enhance the Walker circulation and increase the convergence in the lower troposphere over the warm pool and thus increase vertical motion as well as the total amount of high cloud cover and IWP.

The patterns of major cooling and warming areas in Figures 7d–7f from the low sulfate/low dust cases are similar to the high sulfate/high dust cases. However, there are also some noticeable differences. Since the ice number from homogeneous freezing is much smaller in the $L_{sulf}L_{dust}$ case, the inhibition of homogeneous freezing by the aircraft soot IN renders a smaller decrease of ice particle number. In areas with both heterogeneous freezing and homogeneous freezing, we even see increases of ice numbers when the ice number from the increased heterogeneous freezing is more than the loss of ice particles due to the inhibited homogeneous freezing. As a result, the regions of cooling for the $L_{sulf}L_{dust}$ case in Figure 7e occupy a smaller geographical extent than those in the $H_{sulf}H_{dust}$ case shown in Figure 7b. Case $L_{sulf}L_{dust}$ also shows a positive long-wave forcing in the Arctic. The global mean long-wave forcing is approximately a factor of 3 different in the two cases, $-1.12\,W\,m^{-2}$ in case $H_{sulf}H_{dust}$ and $-0.32\,W\,m^{-2}$ in case $L_{sulf}L_{dust}$. The short-wave forcing is also larger in the $H_{sulf}H_{dust}$ case than that in the $L_{sulf}L_{dust}$ case ($+0.82\,W\,m^{-2}$ versus $+0.41\,W\,m^{-2}$). However, the difference is smaller than that of the long-wave radiative forcing by a factor of 2. This is because even though case $H_{sulf}H_{dust}$ shows a larger decrease of IWP at the middle to high latitudes in the NH, unlike the long-wave radiative forcing, whose cooling effect is not directly affected by the incoming solar radiation, the short-wave radiative forcing shows a smaller warming effect at high latitudes due to decreased incoming solar radiation. As a result, the global radiative forcing (long-wave forcing + short-wave forcing) is negative for the $H_{sulf}H_{dust}$ case, $-0.29\,W\,m^{-2}$, but positive for the $L_{sulf}L_{dust}$ case, $+0.09\,W\,m^{-2}$.

Figure 8 shows the changes of IWP and net all-sky total radiative forcing at the TOA from the two pure heterogeneous freezing cases. As expected, without inhibition of homogeneous freezing, there is an increase of IWP in both cases in areas with a large ratio of aircraft soot to dust: in the region from the U.S. to Europe and in East/South/Southeast Asia. The patterns of the total radiative forcing at the TOA closely resemble those of the IWP changes. The global mean change in both the IWP and the total radiative forcing is positive. Since the Het_L_{dust} case has a larger ratio of aircraft soot to dust concentration, it has a larger increase in IWP and a stronger global mean radiative forcing ($+0.21\,W\,m^{-2}$ versus $+0.11\,W\,m^{-2}$ in case Het_H_{dust}).

Table 3 summarizes the global average change in the basic cloud and radiative properties for all six cases. Due to the larger ratio of aircraft soot IN to dust number concentration in case $H_{sulf}L_{dust}$ compared to that in case $H_{sulf}H_{dust}$ and thus the more frequent suppression of homogeneous freezing, case $H_{sulf}L_{dust}$ has larger magnitudes of each property in the table. It also has a more negative global total radiative forcing, $-0.35\ Wm^{-2}$. Case $L_{sulf}H_{dust}$, which has a smaller aircraft soot IN to dust ratio than that in case $L_{sulf}L_{dust}$, results in smaller changes in IWP and all-sky radiative forcing than those in case $L_{sulf}L_{dust}$. The global mean total radiative forcing, which is the sum of two larger forcings of opposite signs (long-wave forcing and short-wave forcing), is less sensitive for the two low sulfate number cases and are both $+0.09\,W\,m^{-2}$.

3.3. Impact of a Larger Ice Nucleating Efficiency

Above, we assumed that only those particles that had previously been incorporated within persistent ice contrails would act as efficient ice nuclei. However, there are many more contrails formed than only those which persist beyond a few hours. Here we also tested the impact of assuming that 20% of all aircraft-emitted soots can act as potential IN. Moreover, we also assumed that the ice nucleating efficiency of these potential IN is not affected by the presence of a coating by sulfate. This latter assumption is motivated by experimental findings of Edwards et al. [1970], which show that coating by NaCl does not alter the preactivation behavior of organic aerosols. The forcings have similar regional patterns to the cases with only ~0.6% of aircraft soot as heterogeneous IN but have much larger magnitudes. The global averaged total radiative forcings also show negative and positive signs depending on the sulfate numbers used for homogeneous freezing but with a much wider range: from $-0.71\,W\,m^{-2}$ (case $H_{sulf}L_{dust}$) to $+0.81\,W\,m^{-2}$

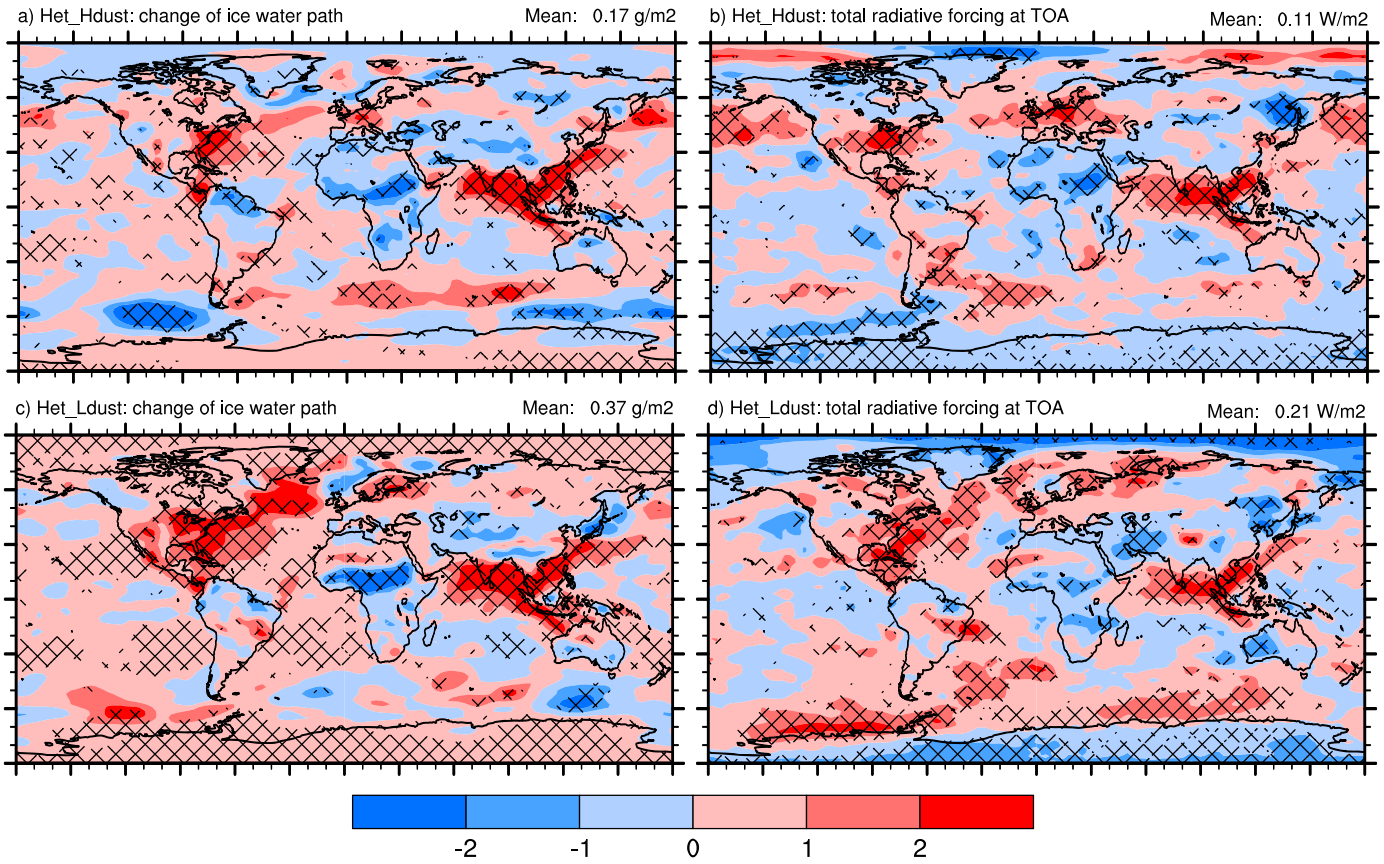

Figure 8. Change in (left) the annual mean ice water path and (right) the all-sky total radiative forcings at the TOA after adding ~0.6% of aircraft soot as IN while assuming a heterogeneous freezing only background for ice clouds. The top graphs are from the high dust cases, and the bottom graphs are from the low dust cases. Differences significant at the 90% level of the Student's *t* test are depicted by meshes.

(case $L_{sulf}L_{dust}$). Table 4 gives a summary of the global average changes in the cloud and radiative properties. Compared to the changes in Table 3, there are several noticeable differences in addition to the much larger overall magnitudes of the all-sky forcings. The clear-sky long-wave forcings are considerably more negative than those in Table 3 due to a larger decrease of water vapor in the tropics in cases $H_{sulf}H_{dust}$ and

Table 3. Global Average Changes and Standard Deviations of the Annual Mean Changes in the Basic Cloud and Radiative Properties When ~0.6% of the Total Aircraft Soot Loading Acts as IN[a]

	$H_{sulf}L_{dust}$	$H_{sulf}H_{dust}$	$L_{sulf}L_{dust}$	$L_{sulf}H_{dust}$	Het_H_{dust}	Het_L_{dust}
ΔCF (W m^{-2})	−0.23 ± 0.22	−0.19 ± 0.21	0.10 ± 0.18	0.09 ± 0.19	0.24 ± 0.17	0.55 ± 0.19
ΔSWCF (W m^{-2})	1.36 ± 0.22	0.85 ± 0.27	0.42 ± 0.19	0.21 ± 0.21	−0.10 ± 0.17	−0.30 ± 0.18
ΔLWCF (W m^{-2})	−1.59 ± 0.17	−1.04 ± 0.20	−0.33 ± 0.11	−0.12 ± 0.14	0.34 ± 0.15	0.86 ± 0.09
ΔFNT (W m^{-2})	−0.35 ± 0.31	−0.29 ± 0.30	0.09 ± 0.27	0.09 ± 0.26	0.11 ± 0.36	0.21 ± 0.34
ΔFSNT (W m^{-2})	1.33 ± 0.23	0.83 ± 0.28	0.41 ± 0.21	0.23 ± 0.23	−0.11 ± 0.23	−0.41 ± 0.23
ΔFLNT (W m^{-2})	−1.68 ± 0.30	−1.12 ± 0.27	−0.32 ± 0.24	−0.14 ± 0.23	0.21 ± 0.25	0.62 ± 0.20
ΔFSNTC (W m^{-2})	−0.03 ± 0.13	−0.03 ± 0.12	−0.01 ± 0.12	0.02 ± 0.09	0.01 ± 0.14	−0.07 ± 0.12
ΔFLNTC (W m^{-2})	−0.10 ± 0.18	−0.07 ± 0.13	0.01 ± 0.16	−0.02 ± 0.14	−0.13 ± 0.17	−0.26 ± 0.13
ΔIWP (g m^{-2})	−0.87 ± 0.17	−0.53 ± 0.15	−0.23 ± 0.12	−0.08 ± 0.16	0.17 ± 0.18	0.37 ± 0.16
ΔLWP (g m^{-2})	−0.55 ± 0.37	−0.28 ± 0.35	−0.25 ± 0.35	−0.16 ± 0.39	−0.15 ± 0.3	−0.07 ± 0.35
ΔTMQ (kg m^{-2})	−0.25 ± 0.08	−0.16 ± 0.09	−0.09 ± 0.08	−0.05 ± 0.08	0.06 ± 0.07	0.13 ± 0.08

[a]CF: total cloud forcing, SWCF: short-wave cloud forcing, LWCF: long-wave cloud forcing, FNT: sum of short- and long-wave fluxes at the TOA, FSNT: all-sky short-wave fluxes at the TOA, FLNT: all-sky long-wave flux at the TOA, FSNTC: clear-sky short-wave flux at the TOA, FLNTC: clear-sky long-wave flux at the TOA, IWP: grid box averaged ice water path, LWP: grid box averaged liquid water path, and TMQ: vertically integrated water vapor.

Table 4. Global Average Change in the Basic Cloud and Radiative Properties When 20% of the Total Aircraft Soot Loading Acts as IN[a]

	$H_{sulf}L_{dust}$	$H_{sulf}H_{dust}$	$L_{sulf}L_{dust}$	$L_{sulf}H_{dust}$
ΔCF (W m^{-2})	−0.09 ± 0.22	0.06 ± 0.25	1.04 ± 0.12	0.83 ± 0.20
ΔSWCF (W m^{-2})	2.88 ± 0.29	1.76 ± 0.24	−0.89 ± 0.20	−1.08 ± 0.22
ΔLWCF (W m^{-2})	−2.97 ± 0.15	−1.70 ± 0.18	1.92 ± 0.14	1.91 ± 0.13
ΔFNT (W m^{-2})	−0.70 ± 0.21	−0.30 ± 0.32	0.80 ± 0.18	0.81 ± 0.30
ΔFSNT (W m^{-2})	2.82 ± 0.28	1.66 ± 0.25	−0.82 ± 0.18	−1.03 ± 0.23
ΔFLNT (W m^{-2})	−3.52 ± 0.25	−2.96 ± 0.27	1.63 ± 0.22	1.84 ± 0.22
ΔFSNTC (W m^{-2})	−0.06 ± 0.08	−0.09 ± 0.14	0.06 ± 0.15	0.05 ± 0.14
ΔFLNTC (W m^{-2})	−0.55 ± 0.15	−0.30 ± 0.16	−0.27 ± 0.15	−0.07 ± 0.15
ΔIWP (g m^{-2})	−1.05 ± 0.15	−0.27 ± 0.13	1.57 ± 0.15	1.57 ± 0.12
ΔLWP (g m^{-2})	−1.02 ± 0.49	−0.41 ± 0.42	0.15 ± 0.38	0.29 ± 0.40
ΔTMQ (kg m^{-2})	−0.59 ± 0.10	−0.37 ± 0.08	0.07 ± 0.09	0.08 ± 0.06

[a]See Table 3 for the definition of each quantity.

$H_{sulf}L_{dust}$ The changes in the IWP and the LWP are now positive in cases $L_{sulf}L_{dust}$ and $L_{sulf}H_{dust}$, since the increases in the IWP and the LWP in the NH outweigh the decreases in the IWP and the LWP in the tropics and SH. The all-sky short-wave radiative forcing, long-wave radiative forcing, and the total radiative forcing at the TOA are presented in Figure S3 in the supporting information. A net warming effect can be observed in most parts of the NH with a net cooling effect over the ocean in the tropics and in the southern hemisphere.

4. Conclusions and Discussion

We used the coupled CAM5/IMPACT model to study the impact of aircraft soot as a potential heterogeneous ice nuclei (IN) on large-scale cirrus cloud. We followed the formation of contrail cirrus and assumed that aircraft soot particles that have been frozen within contrails are preactivated and are good IN unless three or more monolayers of sulfate are coated on them. Approximately 8% of the total aircraft soot is shown to be incorporated within the persistent contrail cirrus. If a sulfate coating (of three monolayers) on the aircraft soot is able to reduce their effectiveness as heterogeneous IN, the actual amount of aircraft soot particles that are able to potentially serve as IN is only ~0.6% of the total aircraft soot suspended in the air. We then simulated the climate impact of this aircraft soot acting as heterogeneous ice nuclei in cirrus clouds. We varied the background sulfate and dust numbers used in the ice nucleation parameterization because of the variations on how this is treated within the current literature.

If aircraft soot emissions provide additional IN, they reduce the occurrence of homogeneous freezing and reduce the ice number in regions, where the background is dominated by homogeneous freezing. This has a net cooling effect at the top of the atmosphere over the tropical Indian Ocean, Central America, and the North Atlantic Ocean, where the background is dominated by homogeneous freezing. Over Africa and the Middle East to Central Asia, where the background atmosphere is dominated by the heterogeneous freezing, aircraft soot increases the ice number and ice water path and thus has a net warming effect at the top of the atmosphere. These results are consistent with those presented by *Hendricks et al*. [2005]. We find however that the sign of the net global radiative forcing at the top of the atmosphere is sensitive to the sulfate numbers used for homogeneous freezing. A large sulfate number leads to a larger decrease of ice number when homogeneous freezing is inhibited by the addition of aircraft soot. Thus, the two high sulfate number cases, $H_{sulf}H_{dust}$ and $H_{sulf}L_{dust}$, show a more negative global mean long-wave radiative forcing (−1.12 W m^{-2} and −1.68 W m^{-2}) at the top of the atmosphere and have a net global cooling effect (−0.29 W m^{-2} and −0.35 W m^{-2}). In the two low sulfate number cases, $L_{sulf}L_{dust}$ and $L_{sulf}H_{dust}$, the global mean long-wave forcing is also negative but smaller in magnitude (−0.32 W m^{-2} and −0.14 W m^{-2}, respectively). A decrease in the IWP causes a warming effect in the short-wave radiation, which outweighs the cooling effect in the long-wave radiation and leads to a net global warming effect (+0.09 W m^{-2} for both cases). The short- and long-wave radiative forcings are also sensitive to the dust numbers. Aircraft soot IN show larger impacts in both long- and short-wave radiative forcings when the dust number is smaller, but the smaller dust number does not change the sign of the global mean total radiative forcing.

In this study, major cooling takes place over Central America and the tropical Indian Ocean since these are regions where aircraft soot reduces the occurrence of homogeneous freezing. Recent studies based on in situ observations suggest that ice number concentrations are low near the tropical tropopause and that heterogeneous freezing is more likely to be the predominant freezing process [*Murray et al*., 2010; *Jensen et al*., 2013]. *Cziczo et al*. [2013] suggests that heterogeneous freezing is also the predominant freezing process in both anvil cirrus from convective outflow and synoptically formed cirrus clouds observed between 5 km and 16 km. Different mechanisms including glassy organic aerosols [*Jensen et al*., 2010; *Murray et al*., 2010], dynamic balance [*Barahona and Nenes*, 2011], preexisting ice [*Kuebbeler et al*., 2014], and slow large-scale movement [*Spichtinger and Krämer*, 2012] have been proposed to explain the observed low ice number concentration. To explore the possible upper limit of the aircraft soot forcings, we conducted two sensitivity tests, cases Het_H_{dust} and Het_L_{dust}, which assume that all freezing takes place heterogeneously. In these cases, aircraft soot increases the IWP and has a net warming effect over regions with high aircraft soot emissions leading to a positive global mean forcing (+0.11 W m^{-2} for the high dust case and +0.21 W m^{-2} for the low dust case). These two forcings may approximate an upper limit for the effect of aircraft soot acting as IN.

In this study, we show that both the magnitude and the sign of the global total radiative forcing from aircraft soot IN can vary because of uncertainties in the treatment of background ice nucleation in the atmosphere. We used a range of sulfate and dust number concentrations to illustrate this, in part because the correct representation for the upper troposphere is not known. In addition, the current model needs to be improved. In our current model setup, we only considered immersion freezing while deposition freezing was not included. The model also does not include consideration of the condensation of water vapor onto preexisting ice prior to and during the freezing of new particles. The upper bound on the value of the subgrid scale updraft velocity is another important uncertainty. When we increase the upper bound from 0.2 m s^{-1} to 0.3 m s^{-1}, there is more homogeneous freezing in the background atmosphere and less suppression of homogeneous freezing when aircraft soot is added. As a result, the forcing associated with the addition of aircraft soot has a smaller magnitude (−0.03 W m^{-2} in case $H_{sulf}H_{dust}$ and −0.01 W m^{-2} in case $L_{sulf}L_{dust}$).

Moreover, there are additional uncertainties caused by whether or not preactivated aircraft soot acts as potential IN and whether or not sulfate coatings cause this IN capability to cease. There are no observations to directly support assumptions for the ice nucleating efficiency of preactivated aircraft soot, so the forcings presented here primarily demonstrate the magnitude of uncertainty forcing caused by adding IN to background atmospheres with different treatments for homogeneous and heterogeneous aerosol ice nucleating efficiency. Moreover, if the actual effectiveness of aircraft soot acting as IN is smaller than the fraction in this study, the calculated forcing may not be statistically significant as found, for example, in *Gettelman and Chen* [2013]. If the fraction is higher, as we showed in the sensitivity test, the forcings could have a much larger range (−0.70 W m^{-2} to +0.81 W m^{-2}) depending on the background sulfate and dust numbers. Both further laboratory and field experiments are needed to understand the properties of the aircraft soot as heterogeneous IN as well as the effect of the preactivation. Due to the many different combinations of fuel types, engine types, and atmospheric ambient conditions, this will not be an easy task.

Acknowledgments

This work was funded in by NSF project number AGS-0946739. Computer time was provided by the NCAR CISL facility. This work benefited to a significant extent by previous work funded by the Department of Transportation's Aviation Climate Change Research Initiative under contract DTRT57-10-C-10011. Data supporting all the figures in the present paper are available through the correspondence author (Cheng Zhou, zhouc@umich.edu).

References

Adler, G., T. Koop, C. Haspel, I. Taraniuk, T. Moise, I. Koren, R. H. Heiblum, and Y. Rudich (2013), Formation of highly porous aerosol particles by atmospheric freeze-drying in ice clouds, *Proc. Natl. Acad. Sci. U.S.A.*, *110*(51), 20,414–20,419.

Appleman, H. (1953), The formation of exhaust condensation trails by jet aircraft, *Bull. Am. Meteorol. Soc.*, *34*, 14–20.

Barahona, D., and A. Nenes (2011), Dynamical states of low temperature cirrus, *Atmos. Chem. Phys.*, *11*, 3757–3771, doi:10.5194/acp-11-3757-2011.

Barrett, S., et al. (2010), Guidance on the use of AEDT gridded aircraft emissions in atmospheric models, version 2.0, *Tech. Rep.*, Federal Aviation Administration.

Burkhardt, U., and B. Kärcher (2011), Global radiative forcing from contrail cirrus, *Nat. Clim. Change*, *1*, 54–58, doi:10.1038/nclimate1068.

Chen, C.-C., A. Gettelman, C. Craig, P. Minnis, and D. P. Duda (2012), Global contrail coverage simulated by CAM5 with the inventory of 2006 global aircraft emissions, *J. Adv. Model. Earth Syst.*, *4*, M04003, doi:10.1029/2011MS000105.

Cziczo, D. J., K. D. Froyd, S. J. Gallavardin, O. Moehler, S. Benz, H. Saathoff, and D. M. Murphy (2009), Deactivation of ice nuclei due to atmospherically relevant surface coatings, *Environ. Res. Lett.*, *4*, 044013, doi:10.1088/1748-9326/4/4/044013.

Cziczo, D. J., K. D. Froyd, C. Hoose, E. J. Jensen, M. Diao, M. A. Zondlo, J. B. Smith, C. H. Twohy, and D. M. Murphy (2013), Clarifying the dominant sources and mechanisms of cirrus cloud formation, *Science*, *340*(6138), 1320–1324.

Duda, D. P., P. Minnis, K. Khlopenkov, T. L. Chee, and R. Boeke (2013), Estimation of 2006 Northern Hemisphere contrail coverage using MODIS data, *Geophys. Res. Lett.*, *40*, 612–617, doi:10.1002/grl.50097.

Edwards, G. R., L. F. Evans, and A. F. Zipper (1970), Two-dimensional phase changes in water adsorbed on ice-nucleating substrates, *Trans. Faraday Soc.*, *66*, 220–234.

Evans, L. F. (1967), Two-dimensional nucleation of ice, *Nature*, *213*, 384–385.
Gettelman, A., and C. Chen (2013), The climate impact of aviation aerosols, *Geophys. Res. Lett.*, *40*, 2785–2789, doi:10.1002/grl.50520.
Gettelman, A., X. Liu, S. J. Ghan, H. Morrison, S. Park, A. J. Conley, S. A. Klein, J. Boyle, D. L. Mitchell, and J.-L. F. Li (2010), Global simulations of ice nucleation and ice supersaturation with an improved cloud scheme in the community atmosphere model, *J. Geophys. Res.*, *115*, D18216, doi:10.1029/2009JD013797.
Gettelman, A., X. Liu, D. Barahona, U. Lohmann, and C. Chen (2012), Climate impacts of ice nucleation, *J. Geophys. Res.*, *117*, D20201, doi:10.1029/2012JD017950.
Hendricks, J., B. Kärcher, U. Lohmann, and M. Ponater (2005), Do aircraft black carbon emissions affect cirrus clouds on the global scale?, *Geophys. Res. Lett.*, *32*, L12814, doi:10.1029/2005GL022740.
Hendricks, J., B. Kärcher, and U. Lohmann (2011), Effects of ice nuclei on cirrus clouds in a global climate model, *J. Geophys. Res.*, *116*, D18206, doi:10.1029/2010JD015302.
Jensen, E. J., et al. (2009), On the importance of small ice crystals in tropical anvil cirrus, *Atmos. Chem. Phys.*, *9*, 5519–5537, doi:10.5194/acp-9-5519-2009.
Jensen, E. J., L. Pfister, T.-P. Bui, P. Lawson, and D. Baumgardner (2010), Ice nucleation and cloud microphysical properties in tropical tropopause layer cirrus, *Atmos. Chem. Phys.*, *10*, 1369–1384, doi:10.5194/acp-10-1369-2010.
Jensen, E. J., G. Diskin, R. P. Lawson, S. Lance, T. P. Bui, D. Hlavka, M. McGill, L. Pfister, O. B. Toon, and R. Gao (2013), Ice nucleation and dehydration in the Tropical Tropopause Layer, *Proc. Natl. Acad. Sci. U.S.A.*, *110*, 2041–2046, doi:10.1073/pnas.1217104110.
Kärcher, B., and J. Ström (2003), The roles of dynamical variability and aerosols in cirrus cloud formation, *Atmos. Chem. Phys.*, *3*, 823–838, doi:10.5194/acp-3-823-2003.
Kärcher, B., O. Möhler, P. J. DeMott, S. Pechtl, and S. Yu (2007), Insights into the role of soot aerosols in cirrus cloud formation, *Atmos. Chem. Phys.*, *7*, 4203–4227.
Koehler, K. A., P. J. DeMott, S. M. Kreidenweis, O. B. Popovicheva, M. D. Petters, C. M. Carrico, E. D. Kireeva, T. D. Khokhlova, and N. K. Shonija (2009), Cloud condensation nuclei and ice nucleation activity of hydrophobic and hydrophilic soot particles, *Phys. Chem. Chem. Phys.*, *11*, 7906–7920.
Krämer, M., et al. (2009), Ice supersaturations and cirrus cloud crystal numbers, *Atmos. Chem. Phys.*, *9*, 3505–3522, doi:10.5194/acp-9-3505-2009.
Kuebbeler, M., U. Lohmann, J. Hendricks, and B. Kärcher (2014), Dust ice nuclei effects on cirrus clouds, *Atmos. Chem. Phys.*, *14*, 3027–3046, doi:10.5194/acp-14-3027-2014.
Lee, D. S., D. W. Fahey, P. M. Forster, P. J. Newton, R. C. N. Wit, L. L. Lim, B. Owen, and R. Sausen (2009), Aviation and global climate change in the 21st century, *Atmos. Env.*, *43*, 3520–3537, doi:10.1016/j.atmosenv.2009.04.024.
Liu, X., and J. E. Penner (2005), Ice nucleation parameterization for global models, *Meteorol. Z.*, *14*, 499–514.
Liu, X., J. E. Penner, S. J. Ghan, and M. Wang (2007), Inclusion of ice microphysics in the NCAR Community Atmosphere Model version 3 (CAM3), *J. Clim.*, *20*, 4526–4547.
Liu, X., et al. (2012a), Towards a minimal representation of aerosol direct and indirect effects: Model description and evaluation, *Geosci. Model Dev.*, *5*, 709–735, doi:10.5194/gmd-4-709-2012.
Liu, X., X. Shi, K. Zhang, E. J. Jensen, A. Gettelman, D. Barahona, A. Nenes, and P. Lawson (2012b), Sensitivity studies of dust ice nuclei effect on cirrus clouds with the Community Atmosphere Model CAM5, *Atmos. Chem. Phys.*, *12*, 12,061–12,079, doi:10.5194/acp-12-12061-2012.
Minnis, P., D. F. Young, D. P. Garber, L. Nguyen, W. L. Smith Jr., and R. Palikonda (1998), Transformation of contrails into cirrus during SUCCESS, *Geophys. Res. Lett.*, *25*, 1157–1160, doi:10.1029/97GL03314.
Minnis, P., S. T. Bedka, D. P. Duda, K. M. Bedka, T. Chee, J. K. Ayers, R. Palikonda, D. A. Spangenberg, K. V. Khlopenkov, and R. Boeke (2013), Linear contrail and contrail cirrus properties determined from satellite data, *Geophys. Res. Lett.*, *40*, 3220–3226, doi:10.1002/grl.50569.
Möhler, O., et al. (2006), Efficiency of the deposition mode ice nucleation on mineral dust particles, *Atmos. Chem. Phys.*, *6*(10), 3007–3021.
Möhler, O., et al. (2008), The effect of organic coating on the heterogeneous ice nucleation efficiency of mineral dust aerosols, *Environ. Res. Lett.*, *3*(2), 025007, doi:10.1088/1748-9326/3/2/025007.
Murray, B. J., et al. (2010), Heterogeneous nucleation of ice particles on glassy aerosols under cirrus conditions, *Nat. Geosci.*, *3*, 233–237.
Penner, J. E., Y. Chen, M. Wang, and X. Liu (2009), Possible influence of anthropogenic aerosols on cirrus clouds and anthropogenic forcing, *Atmos. Chem. Phys.*, *9*, 879–896, doi:10.5194/acp-9-879-2009.
Rogers, D. C., P. J. DeMott, S. M. Kreidenweis, and Y. Chen (1998), Measurements of ice nucleating aerosols during SUCCESS, *Geophys. Res. Lett.*, *25*, 1383–1386, doi:10.1029/97GL03478.
Schmidt, E. (1941), Die Entstehung von Eisnebel aus den Auspuffgasen von Flugmotoren, *Schr. Dtsch. Akad. Luftfahrtforsch.*, *44*, 1–15.
Schumann, U. (1996), On conditions for contrail formation from aircraft exhausts, *Meteorol. Z.*, *5*, 4–24.
Schumann, U., and K. Graf (2013), Aviation-induced cirrus and radiation changes at diurnal timescales, *J. Geophys. Res. Atmos.*, *118*, 2404–2421, doi:10.1002/jgrd.50184.
Spangenberg, D. A., P. Minnis, S. T. Bedka, R. Palikonda, D. P. Duda, and F. G. Rose (2013), Contrail radiative forcing over the Northern Hemisphere from 2006 Aqua MODIS data, *Geophys. Res. Lett.*, *40*, 595–600, doi:10.1002/grl.50168.
Spichtinger, P., and M. Krämer (2012), Tropical tropopause ice clouds: A dynamic approach to the mystery of low crystal numbers, *Atmos. Chem. Phys. Discuss.*, *12*, 28,109–28,153, doi:10.5194/acpd-12-28109-2012.
Wagner, R., O. Möhler, H. Saathoff, M. Schnaiter, J. Skrotzki, T. Leisner, T. W. Wilson, T. L. Malkin, and B. J. Murray (2012), Ice cloud processing of ultra-viscous/glassy aerosol particles leads to enhanced ice nucleation ability, *Atmos. Chem. Phys.*, *12*, 8589–8610, doi:10.5194/acp-12-8589-2012.
Welti, A., F. Lüönd, O. Stetzer, and U. Lohmann (2009), Influence of particle size on the ice nucleating ability of mineral dusts, *Atmos. Chem. Phys.*, *9*(18), 6705–6715, doi:10.5194/acp-9-6705-2009.
Yi, B., P. Yang, K.-N. Liou, P. Minnis, and J. E. Penner (2012), Simulation of the global contrail radiative forcing: A sensitivity analysis, *Geophys. Res. Lett.*, *39*, L00F03, doi:10.1029/2012GL054042.
Zhang, K., X. Liu, M. Wang, J. M. Comstock, D. L. Mitchell, S. Mishra, and G. G. Mace (2013), Evaluating and constraining ice cloud parameterizations in CAM5 using aircraft measurements from the SPARTICUS campaign, *Atmos. Chem. Phys.*, *13*, 4963–4982, doi:10.5194/acp-13-4963-2013.
Zhou, C., J. E. Penner, Y. Ming, and X. L. Huang (2012), Aerosol forcing based on CAM5 and AM3 meteorological fields, *Atmos. Chem. Phys.*, *12*, 9629–9652, doi:10.5194/acp-12-9629-2012.